# REPORT DOCUMENTATION PAGE

Form Approved OMB No. 0704-0188



| 1. REPORT DATE *(DD-MM-YYYY)* | 2. REPORT TYPE | 3. DATES COVERED *(From – To)* |
|---|---|---|
| 01-12-2003 | Final Report | 26 September 2002 - 26-Sep-03 |

**4. TITLE AND SUBTITLE**

Characterization of the Microstructure of fine Energetic Materials

**5a. CONTRACT NUMBER**
FA8655-02-M4066

**5b. GRANT NUMBER**

**5c. PROGRAM ELEMENT NUMBER**

**6. AUTHOR(S)**

Dr. Michael J Herrmann

**5d. PROJECT NUMBER**

**5d. TASK NUMBER**

**5e. WORK UNIT NUMBER**

**7. PERFORMING ORGANIZATION NAME(S) AND ADDRESS(ES)**

Fraunhofer Institut für Chemische Technologie
J.-v.-Fraunhoferstraße 7
Pfinztal 76327
Germany

**8. PERFORMING ORGANIZATION REPORT NUMBER**
N/A

**9. SPONSORING/MONITORING AGENCY NAME(S) AND ADDRESS(ES)**

EOARD
PSC 802 BOX 14
FPO 09499-0014

**10. SPONSOR/MONITOR'S ACRONYM(S)**

**11. SPONSOR/MONITOR'S REPORT NUMBER(S)**
SPC 02-4066

**12. DISTRIBUTION/AVAILABILITY STATEMENT**

Approved for public release; distribution is unlimited.

**13. SUPPLEMENTARY NOTES**



**14. ABSTRACT**

This report results from a contract tasking Fraunhofer Institut für Chemische Technologie as follows: Lattice defects in energetic materials will be measured using X-ray diffraction. The method shall be tested for its ability to characterize lattice defects in RDX and HMX, where dislocations gliding and deformation twinning are believed to dominate mechanical behavior. X-ray diffraction patterns will be evaluated relating to phase, residual strain, crystallite size and micro strain. The occurring phases and the lattice parameters of the samples will be determined by Rietveld-method using literature data. Micro strain and crystallite size will be determined with the Williamson Hall method by plotting reciprocal peak widths versus reciprocal lattice distances. New routines for size/strain evaluation, implemented in Rietveld programs will be tested and compared with the Williamson Hall method.

**15. SUBJECT TERMS**
EOARD, Materials, Energetic Materials, Propellants, lattice defects, micro strain

| 16. SECURITY CLASSIFICATION OF: | | | 17. LIMITATION OF ABSTRACT | 18. NUMBER OF PAGES | 19a. NAME OF RESPONSIBLE PERSON |
|---|---|---|---|---|---|
| a. REPORT | b. ABSTRACT | c. THIS PAGE | | | CHARLES H. WARD, Lt Col, USAF |
| UNCLAS | UNCLAS | UNCLAS | UL | 20 | 19b. TELEPHONE NUMBER *(Include area code)* +44 (0)20 7514 3154 |

# Characterization of the Microstructure of fine Energetic Materials

## Final Report

by
Michael Herrmann
November 2003

EUROPEAN OFFICE OF AEROSPACE RESEARCH AND DEVELOPMENT
London, England
Contract Number: FA8655-02-M-4066
September 2003 – September 2004

Contractor:
Fraunhofer Institut für Chemische Technologie
Energetische Materialien
J.-v.-Fraunhofer-Straße 7
76327 Pfinztal / Germany
Principal Investigator: Dr. Michael Herrmann



The Research reported in this document has been made possible through the support and sponsorship of the U.S. Government through its European Office of Aerospace Research and Development

## Summary

Mechanical sensitivity of energetic materials as explosives and propellants has been discussed as a function of particle size and lattice defects originated during crystallization and particle processing. As a conclusive correlation hitherto is difficult to achieve an approach is made to investigate lattice defects using X-ray diffraction.

SEM and X-ray diffraction measurements were carried out with fine RDX and HMX. These materials have the interesting feature that different defect mechanisms are supposed to dominate the mechanical behavior. The X-ray diffraction patterns were evaluated by Rietveld- and peak profile analysis. The X-ray systems has been calibrated using the profile standard SRM 660a from the National Institute for Standards and Technology (NIST).

A new preparation technique was tested in order to reduce broadening due to the low absorption, particularly in energetic materials like nitramines.

The investigations reveal interesting details about lattice defects in energetic materials. Characteristic peak broadening was found for the nitramines RDX and HMX. The results agree with the models described in literature, pointing to a higher micro strain in HMX. The two-dimensional interfaces of twins in HMX seem to create higher micro strain then the one dimensional dislocations in RDX. Besides twin interfaces may divide crystallites into smaller coherently diffracting domains. Moreover an unisotropy peak broadening was found for RDX, which were discussed in terms of strain fields created by unisotropic dislocation.

## List of keywords

Energetic materials, lattice defects, micro strain, X-ray diffraction

## Introduction

Mechanical sensitivity is an important issue for energetic materials as explosives and propellants. It has been discussed as a function of particle size and lattice defects originated during crystallization and particle processing. However, a conclusive correlation was hitherto difficult to achieve, because the integral measurement of defects is difficult. An approach is made to quantify and characterize lattice defects in energetic materials by means of X-ray diffraction.

## State of the art

### X-ray diffraction

The X-ray diffraction allows a characterization of energetic crystals and particles obtained not only from the surface and with point measurements but from a representative volume of a substance. The method is based on the evaluation of diffraction line profiles; their positions, intensities, widths and shapes. The line intensities and positions are generally used to identify and quantify crystalline ingredients or phases, to determine or refine crystal structures or investigate residual strain.

The line widths have many physical sources. The measuring system reveals a geometrical profile representing optical devices and X-ray tube. This profile is broadened by sample features as size, strain, diffuse scattering, misfits between phases, etc. The effects superimpose and often are not easy to separate. Crystal size and lattice distortion broadening are usual present concomitantly, and strain broadening can be caused by many different crystal defects as dislocations, stacking faults, point defects, misfits, distorted grain boundaries, concentration gradients, etc. The Warren-Averbach-method solves the problem of the separation of size and strain broadening revealing the root mean-squared strain ($<\varepsilon^2>^{1/2}$). (Ungar et al. 2000) Williamson and Hall (1953) suggested that the full width at half-maximum (FWHM) of diffraction profiles can be written as the sum of strain and size broadening, which means in terms of reciprocal units: $\beta^*=\Delta K=0.9/D+\Delta K^D$ where $\Delta K^D$ is the strain contribution to peak broadening and $D$ is the average grain size. ($d^*=K=2\lambda \sin\theta$, $\Delta K=2\Delta\theta/\lambda \cos\theta$ with the peak width $\beta$, the lattice spacing $d$, the diffraction angle $\theta$, the half of FWHM $\Delta\theta$ and the wave length $\lambda$)

A crucial point in this method is the physical model placed behind the root-mean-squared strains. If the displacement of atoms or molecules relative to their ideal position is random the root-mean-squared strain is a constant. In most cases, however, strain is caused by dislocations, and in this case the displacements have a well defined spatial distribution and the root-mean-squared strain is far from being constant. Recent results obtained by analyzing strain anisotropy enabled a microscopic model for the root-mean-squared strains based on dislocation theory, called *modified* Warren-Averbach analysis and *modified* Williamson-Hall plot. (Ungar et al. 2000)

Beside the Williamson-Hall method, where strain and size broadening are separated on the basis that size or strain is diffraction order independent or dependent, other methods bases on a profile analysis of single peaks, as the shapes of size and strain components are different (e.g. Manual of TOPAS from Bruker AXS).

For calibration and determination of geometrical profiles powder diffraction standard reference materials are available from the National Institute of Standards and Technology NIST. The line position and line shape standard SRM 660a is especially recommended for size-strain investigations as it is more or less strain-free and yields no size broadening. It consists of a fine Lanthanum Hexaboride powder with aggregates of crystallizes in the 2 to 5 µm range. (NIST 2000).

### Energetics - actual research and structures

According to the discussions mentioned in the introduction concepts were developed to reduce defect concentrations of energetic materials applying careful crystallization and processing methods. Particularly, energetic nitramines as HMX and RDX are in the scope of interest, and for these materials it was shown that an improved internal crystal quality decreases the mechanical sensitivity.

In case of RDX an insensitive industrial product "I-RDX" is already available from SNPE, France. (Bouma et al. 2001, Lécume et al. 2001, Kröber et al. 1998, Van der Heijden et al. 1998).

In order to explain these effects special lattice imperfections are discussed to create hot spots under mechanical stress (Armstrong et al. 1993), and detailed models of embedded defects as dislocations and twins were developed.

*Crystal and real structure of RDX ($C_3H_6N_6O_6$)*

The crystal structure of RDX has been refined from single-crystal neutron-diffraction data by Choi and Prince 1972. The compound crystallizes in the orthorhombic space group Pbca with the lattice parameters a=13.182, b= 11.574 and c=10.709 Å. The elementary cell contains eight RDX molecules, measured and calculated densities amount to 1,816 and 1,806, respectively.

Armstrong and Elban described that the mechanical properties of RDX are explained by the difficulty of moving individual dislocations. Fig. 1 shows the [-100](040) edge dislocation of the RDX lattice, schematically (Armstrong et al.). The dislocation was constructed to explain the (010) slip reported by Cinnick and May in 1969. Later on Elban, Armstrong and colleagues reported the occurrence of slip on (021) and (02-1) systems in RDX.

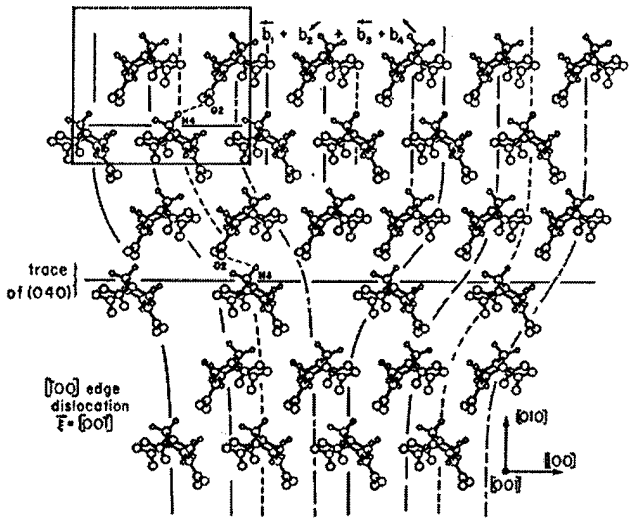


Fig. 1: [-100](400) edge dislocation in RDX, schematically

*Crystal and real structure of HMX ($C_4H_8N_8O_8$)*

HMX crystallizes in four phases; α-, β-, γ- and δ-HMX. β-HMX is the most interesting phase as it is the room temperature stable phase with the highest density. Eiland and Pepinsky found in 1955 space group P21/n with lattice parameters a=6.54, b=11.05, c=7.37 Å and β=102.8°. Reinvestigations by Choi and Boutin in 1970 revealed space group P21/c with the lattice parameters a=6.54, b= 11.05, c=8.70 Å and β=124.3°. The elementary cell contains two molecules, measured and calculated densities amount to 1.894 and 1.90 g/cm$^3$, respectively.

The internal properties of β-HMX seem to be dominated by crystal twinning. Palmer et al. 1982, Cady 1993 and Armstrong et al. 1993 observed (101)-twins in HMX. The twins was found in crystals grown from solutions and when crystals are exhibited to mechanical stress (deformation twinning), and the deformation twinning was found to be reversible at low stress. The twin system is characterized by the specifications $K_1$, $\eta_1$, $K_2$, $\eta_2$ = (101), [10-1], (10-1), [101]. It has been reasoned to be of type II in which the twinning orientation relationship may be visualized to occur by a rotation of 180° about the twinning $\eta_1$ direction, followed by a parallel translation. (Armstrong at al. 1993)

## Objectives and approach

A first approach was made by Engel and Herrmann (2001) with the seed project "Lattice Imperfections of Energetic Materials Measured with X-ray Diffraction" supported by the U.S. Government through its European Research Office of the U.S. Army. Measurements were carried out with relatively large HMX particles crystallized from solutions. The investigations revealed that the method is capable for detecting qualities of coarse crystals, when suited measuring systems are applied to reduce effects of uneven sample surfaces and orientation, and after all show a correlation of micro strain with sensitivity against friction.

With the new project the quantification of micro strain using X-ray diffraction shall be verified especially for fine materials, where effects of uneven surfaces and badly distributed orientations do not appear. Since diffraction peak broadening occurs with small crystallites below a few µm, superimposing with broadening by micro strain, samples with a particle or crystallite size between 20 and one µm shall be used. The characterization of the internal quality shall include the occurring phases, crystallite and particle size, lattice parameters and mean squared micro strain. Particular interest is drawn to the characterization of defect structures. Therefore the unisotropy of micro strain and particle size in RDX and HMX shall be determined and compared with the lattice models described in literature and their orientation.

## Experimental

For the investigations comminuted powders of HMX and RDX with particle sizes of a few microns were provided by the particle processing group of ICT, and samples of the fine powders were investigated under the scanning electron microscopy (SEM) for a first characterization of the crystal quality and morphology.

Diffraction patterns were measured with a diffractometer D5000 from Bruker AXS, equipped with copper tube, vertical soller slits, Ni-kβ-filter, divergence and detector slits of 0,3 ° and 0,1 mm, and rotating sample holder. Tab. 1 summarizes the instrumental parameters and Tab. 7 (Appendix) the diffraction measurements and their conditions. The measurements are designated by X followed by a number, e.g. X3 is the third diffraction measurement with file name mh091203. The measurements will be referred by these numbers in the following chapters. For determining the geometrical profiles of the systems the standard reference material SRM 660a (NIST 2000) was measured under the same conditions as the energetic materials.

A preliminary series was measured with common sample preparation, where the powders were filled up to the edge of a standard sample holder and the surfaces were flattened with a glass plate (X1-X4). Patterns were measured between 5 and 90 °2Theta with a step width of 0.01 °2Theta and a measuring time of 8 s/step (~19h/pattern).

Tab. 1: Instrumental parameters

| Goniometer Radii | Value | Full Axial Model | Value |
|---|---|---|---|
| Primary Radius (mm) | 217.5 | Source Length (mm) | 12 |
| Secondary Radius (mm) | 217.5 | ...Source Width (mm) | 0.04 |
| Equatorial Convolutions | | Sample Length (mm) | 14 |
| RS Width (mm) | 0.1 | RS Length (mm) | 12 |
| FDS Angle (°) | 0.3 / 0.5 | Prim. Soller (°) | 2.3 |
| | | Sec. Soller (°) | 2.3 |

As strong absorption broadening was found with these measurements, particularly with the energetic samples, a second series was started, preparing samples in capillaries on a Debye-Scerrer device (X5-X8), and as thin powder layers prepared on a wafer or an aluminum plate (X9-X16), in order to reduce absorption broadening by reducing the diffracting volume in the sample. The patterns were measured between 10 and 40 °2Theta.

Refined patterns of the powder layers were measured in the reduced 2Theta ranges between 12.5 and 26 °2Theta for RDX, and 14 and 33 °2Theta for HMX and LaB6. Each sample was measured twice, freshly prepared, with 0.005 2Theta step width and 10 s measuring time per step.

## Evaluation

The diffraction patterns measured with the common sample preparation were evaluated using the full pattern fitting tools of the program TOPAS from Bruker/AXS, refining peak positions of so-called hkl-phases calculated from crystal data reported in literature. Peaks were fitted using the ray tracing fundamental parameter approach (FPA), deriving peak profiles from the optical arrangement of the measuring system. Thus phases were identified, peaks were indexed, lattice parameters were refined, and peaks with minimal or without overlap were identified as »single peaks«.

The single peaks were fitted using the split-Pearson VII (SPVII) analytical function and the Fundamental Parameter Approach FPA of program TOPAS.

The evaluation with SPVII yields Full Widths at Half Maximum (FWHM) of the peaks, which were reduced by the geometric peak widths obtained from the standard measurements, in order to obtain pure sample broadening. The data were evaluated in terms of reciprocal units as described by Williamson and Hall. Therefore reciprocal peak widths $\beta^*$ were plotted versus reciprocal lattice distances $d^*$ and linear regression lines were fitted in the low $d^*$-range. The slopes and intercepts of linear regression lines with the y-axis are discussed in terms of micro strain and inverse particle size. Additionally, deviations of the reciprocal peak widths from regression lines were determined and related to their peak indices, and systematic deviations were compared with unisotropic defect models reported in literature.

For the evaluation with the FPA geometrical profiles were parameterized on the basis of the SRM 660a pattern, and the three strongest peaks of each energetic materials pattern were evaluated, revealing a main micro strain and particle size.

The linear absorption coefficients were calculated as described by Klug and Alexander 1974 for an estimation of peak broadening due to low absorption.

## Results

### Particle size and morphology (SEM)

Fig. 2 and Fig. 3 show selected pictures of RDX and HMX obtained with scanning electron microscopy. Both samples consist of particles in the µm-scale. Medium particle sizes may lie between 3 and 5 µm. Comparing the samples, the size distribution of the RDX-particles is narrower, and the surfaces of the RDX-particles are smother and more rounded than those of the HMX-particles.

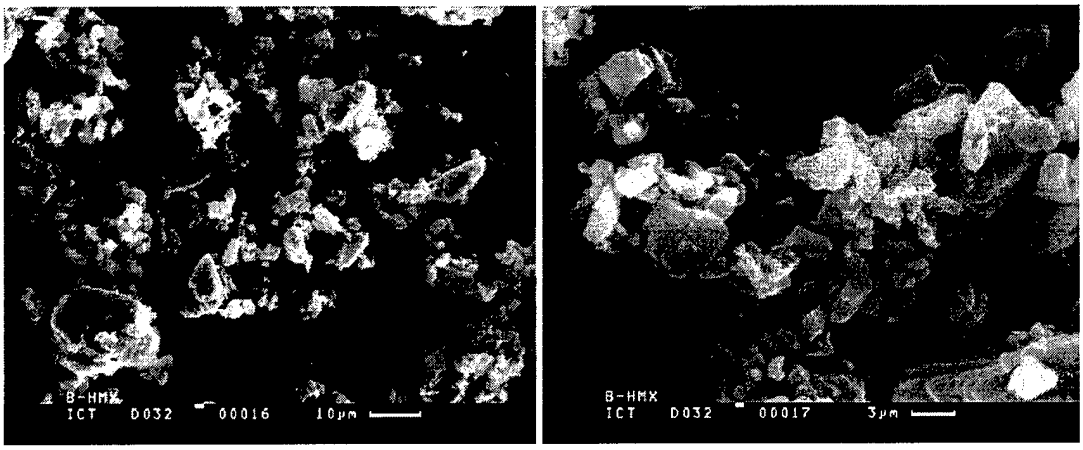


Fig. 2: Selected SEM-pictures of HMX-particles.

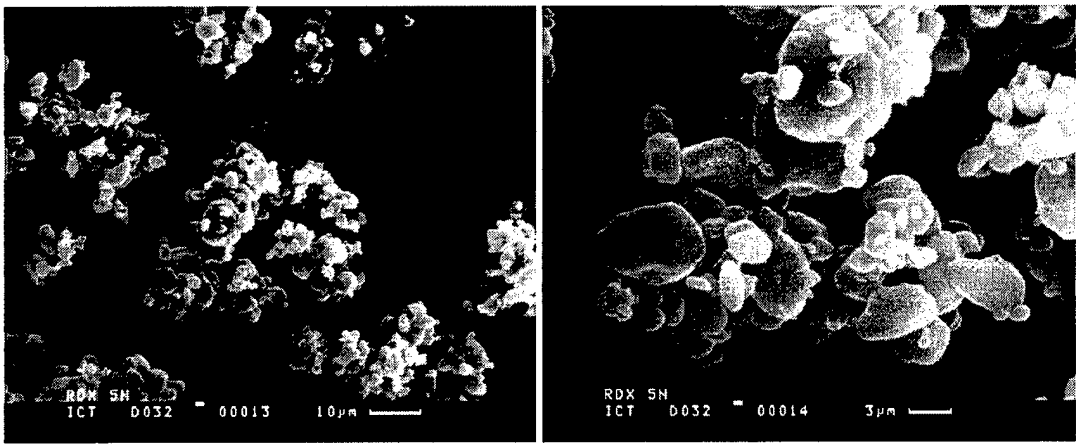


Fig. 3: Selected SEM-pictures of RDX-particles.

## Linear absorption coefficients

The densities, linear absorption coefficients and penetration depths calculated according to Klug and Alexander 1974 are summarized in Tab. 2. The reference material has a much higher absorption coefficient than the energetic materials, resulting in penetration depth of 16 µm for $LaB_6$ and 642 and 614 µm for RDX and HMX, respectively.

Tab. 2: Absorption coefficients and penetration depths for X-ray radiation (CuKα)

| | Density [g/cm$^3$] | Lin. absorption coeff. [1/cm] | Penetration depth [µm] |
|---|---|---|---|
| RDX | 1.82 | 15.6 | 642 |
| HMX | 1.9 | 19.3 | 614 |
| $LaB_6$ (SRM 660a) | 4.711 (ICDD 34-427) | 1098.7 | 9.1 |

## Comparison of measuring techniques

Fig. 4 shows patterns of RDX measured with the Debye-Scherrer device with rotating capillary (X5), and with Bragg-Brentano geometry with common sample preparation (X2) and with powder layers prepared on an aluminum plate (X14). Resulting peak widths for peaks (111) RDX at 13,1 2Theta and (100) $LaB_6$ at 21.35 °2Theta are summarized in Tab. 3.

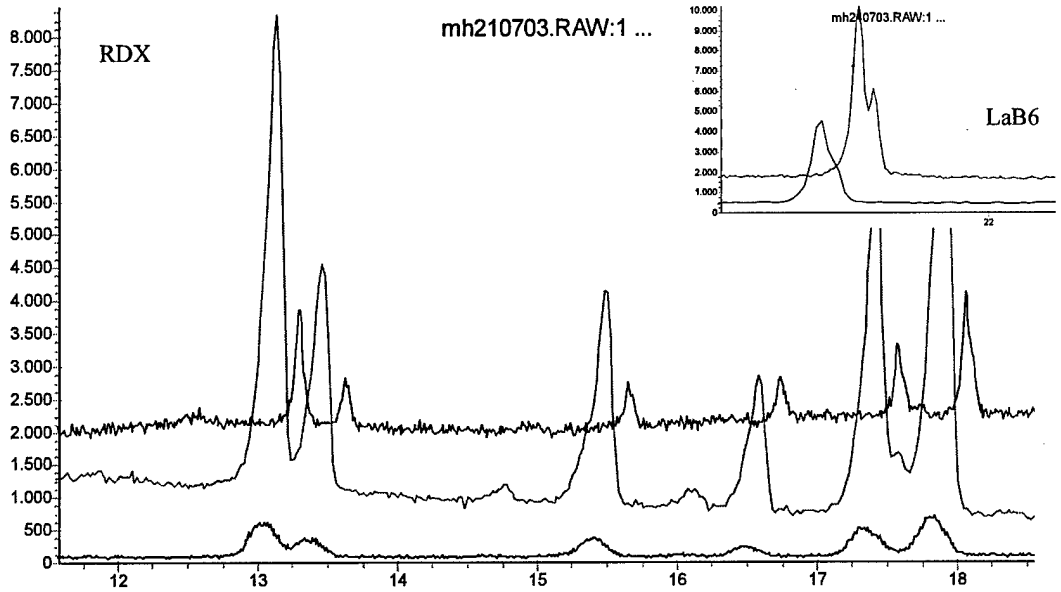


Fig. 4: Diffraction patterns of RDX measured with Debye-Scherrer device (black), Bragg-Brentano with common sample preparation (green) and powder layers on aluminum plate (blue), and of LaB6 (small diagram) measured with common sample preparation (black) and powder layer (blue).

Tab. 3: Peak widths FWHM measured with different systems and preparation techniques

| | $LaB_6$ | RDX |
|---|---|---|
| | (100) at 21.41 °2θ | (111) at 13.07 °2θ |
| Debye-Scherre | | 0.198 |
| Bragg-Brentano | 0.054 | 0.123 |
| Bragg-B., Layer | 0.037 | 0.053 |

The Debye-Scherrer measurements yielded relatively broad peaks widths, e.g. 0.198 °2Theta for (111)RDX, with a low intensity. Narrower peaks were measured with the Bragg-Brentano geometry with 0.123 °2Theta of (111)RDX, and 0.054 °2Theta of (100)$LaB_6$. The narrowest peaks were obtained with the powder layers prepared on an aluminum plate with peak widths of 0.053 of (111)RDX, and even 0.037 °2Theta of (100)$LaB_6$. However, the patterns show also that for the high resolution obtained from powder layers poor peak intensities has to be accepted. Additionally, peak shifts indicate a poor adjustment of the sample position, with the already makeshift preparation technique.

The patterns with the highest intensities obtained with common preparation technique are used for the Rietveld-analysis. For the investigation of peak broadening the measurements with powder layers seem to provide the best basis, if the lack of intensity is compensated by a longer measuring time per step and/or a reduced step size. Besides, selected 2Theta ranges may be measured to limit the required

measuring time per pattern. Fig. 5 shows for instance a pattern X19 (blue) measured with a measuring time of 10 s/0.005 °2Theta. The intensity to underground ratio of this pattern is much better than with the measurement X14 (green) with the shorter measuring time and larger step width.

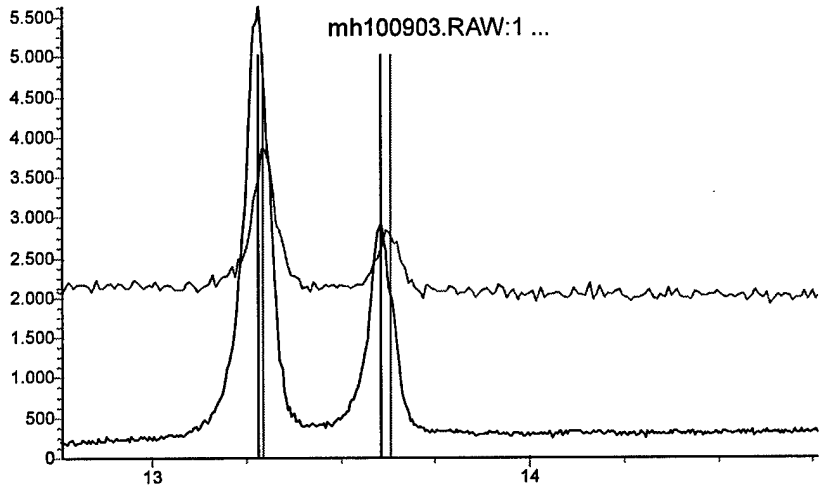


Fig. 5: Diffraction patterns of RDX measured with powder layers and different measuring times and step widths.

## Full pattern fit (XRD-Bragg-Brentano/Rietveld)

Fig. 6 und Fig. 7 show the diffraction patterns X2 of RDX and X1 of HMX and their full pattern fits. All measured peaks belong to the structures of RDX and beta-HMX. However, the RDX-sample contains also HMX indicated by peaks at 14.7 and 16.2 °2Theta.

The refined lattice parameters are summarized in Tab. 4, peak positions and indices in Tab. 9 (Appendix). The Rietveld-analysis yielded good fits of RDX and HMX starting from the data reported by Choi et al. 1972 and Cady at al. 1963. Refined parameters are a=13.205, b=11.616 and c=10.730 Å and a=6.537, b=11.034, c=8.699 Å and β=124.44° for RDX and HMX, respectively. The lattice parameters of RDX seem to be slightly strengthened compared to the literature values, whereas those of HMX agree well with the literature data.

Tab. 4: Lattice parameters obtained by Rietveld-refinement and from literature

| Lattice parameters | RDX | | HMX | |
|---|---|---|---|---|
| | Refinement | Choi et al. 1972 | Refinement | Cady at al. 1963 |
| a [Å] | 13.205 | 13.182 | 6.537 | 6.54 |
| b [Å] | 11.616 | 11.574 | 11.034 | 11.05 |
| c [Å] | 10.730 | 10.709 | 8.699 | 8.70 |
| β [°] | | | 124.44 | 124.3 |

The peak positions and the indexing in Tab. 9 identify separated peaks of RDX at 13.07 (111), 13.40 (200), 16.51 (002), 17.35 (021), 17.83 (102), 20.35 (220), 21.99 (221), 25.35 (131), 30.42 (322), 31.14 (420), and of HMX at 14.70 (011), 18.28 (110), 20.53 (10-2), 22.06 (11-2), 23.02 (120), 27.19 (031), 29.64 (022), 31.90 (13-2), and 33.17 (200). Additionally the RDX-peak (210) at 14.42 °2Theta and the HMX-double peak (11-1)/(020) at 6.02 °2Theta may be used for the evaluation, taking into account

the overlaps. In case of the double peaks the resulting peak widths were reduced by the shift of 0.011 °2Theta between these peaks.

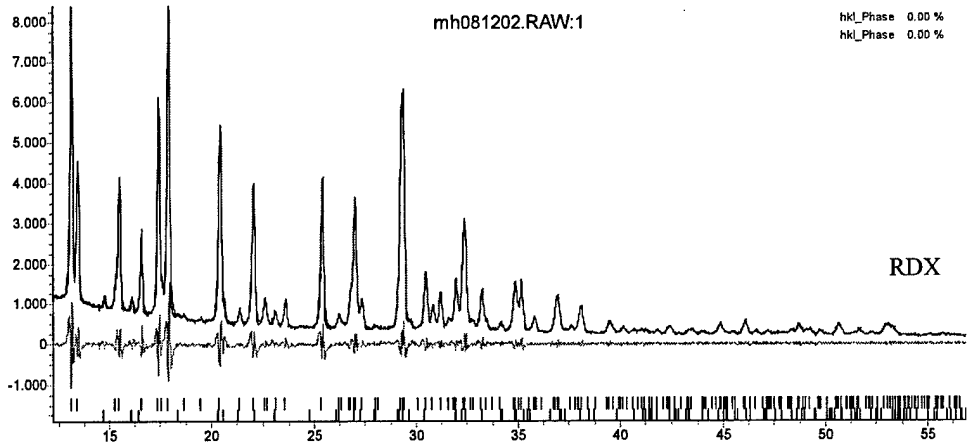


Fig. 6: Diffraction pattern and "hkl-phase fit" of the RDX-sample; positions of RDX and HMX peaks are marked by blue and black bars, respectively.

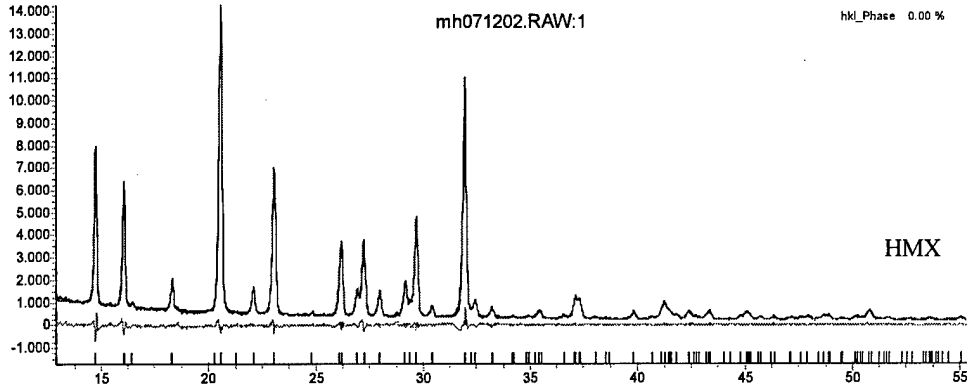


Fig. 7: Diffraction pattern and "hkl-phase fit" of the HMX-sample; all measured peaks belong to HMX.

## Single peak fit

*FWHM of Bragg-Brentano measurements / SPVII-profile*

Fig. 8 till Fig. 10 show selected diffraction peaks of SRM 660a, RDX and HMX fitted by the SPVII analytical function. The calculated fitted well into the measured profiles; particularly, asymmetries of the RDX- and HMX-peaks are simulated accurately by the split function. Compared to the SRM 660a, the energetic materials yield strongly broadened and asymmetric peaks, particularly with common sample preparation.

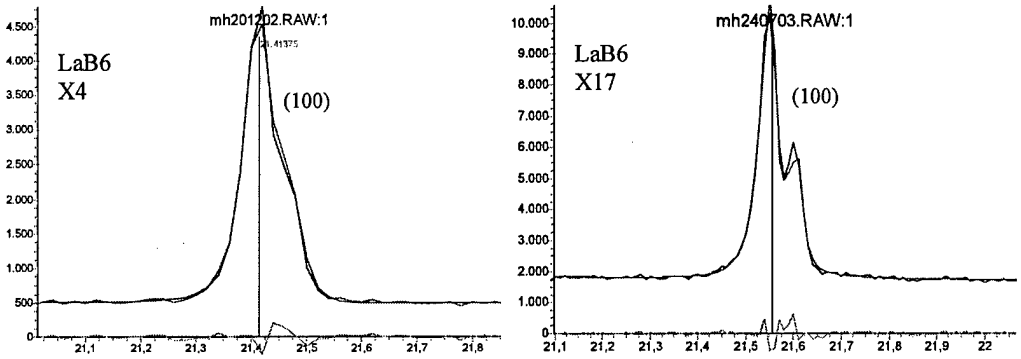


Fig. 8: Diffraction peaks of commonly prepared SRM 660a (left) and a powder layer (right) fitted by SPVII

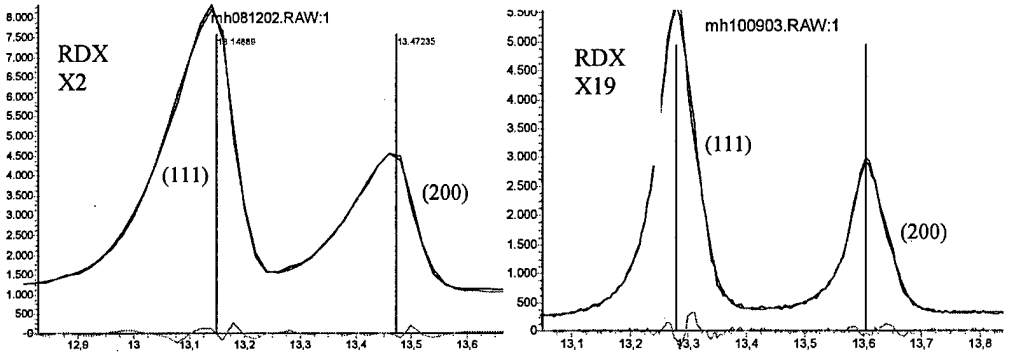


Fig. 9: Diffraction peaks of commonly prepared RDX (left) and a powder layer (right) fitted by SPVII

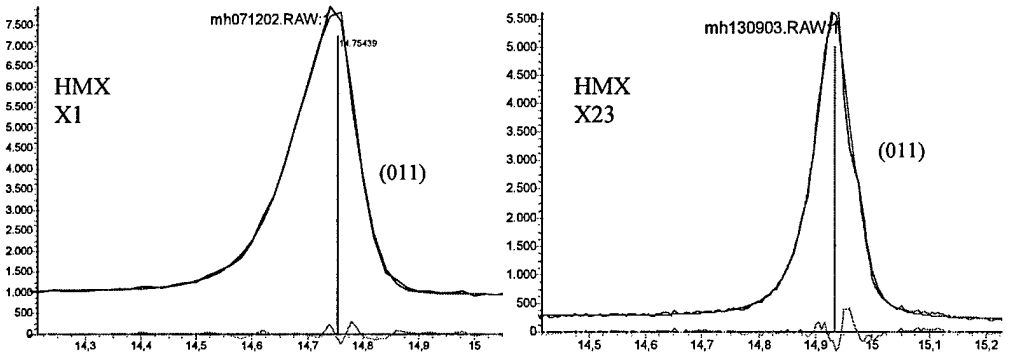


Fig. 10: Diffraction peaks of commonly prepared HMX (left) and a powder layers fitted by the split-Pearson VII analytical function (SPVII)

The fitted peak widths (FWHM) of samples measured with common sample preparation and with powder layers are plotted versus peak position in Fig. 11. It shows interesting details:

With the common preparation technique the peaks of the energetic materials are two to three times wider than those of the standard. The differences represent sample properties as absorption, crystallite size and micro strain.

Using the layer technique peaks of all samples slim down significantly. The effect increases from LaB6 to HMX to RDX, correlating with the calculated penetration depth in Tab. 2. The peak widths of

RDX are nearly as small as those measured with the standard $LaB^6$, indicating that absorption broadening does not more hinder a proper profile analysis.

Comparing the results from powder layers, the peaks of HMX are wider than those of RDX, representing a larger size/strain broadening.

The results are reproducible as shown with the two RDX samples. Additionally, the plot reveals a raw agreement of the runs of the curves measured with both preparation techniques, which give a first idea about the unisotropy of sample properties.

No peaks of SRM 660a appear below 21.4° 2Theta (a reference material for the low 2Theta range should be used for a more accurate determination of geometric peak profiles and widths)

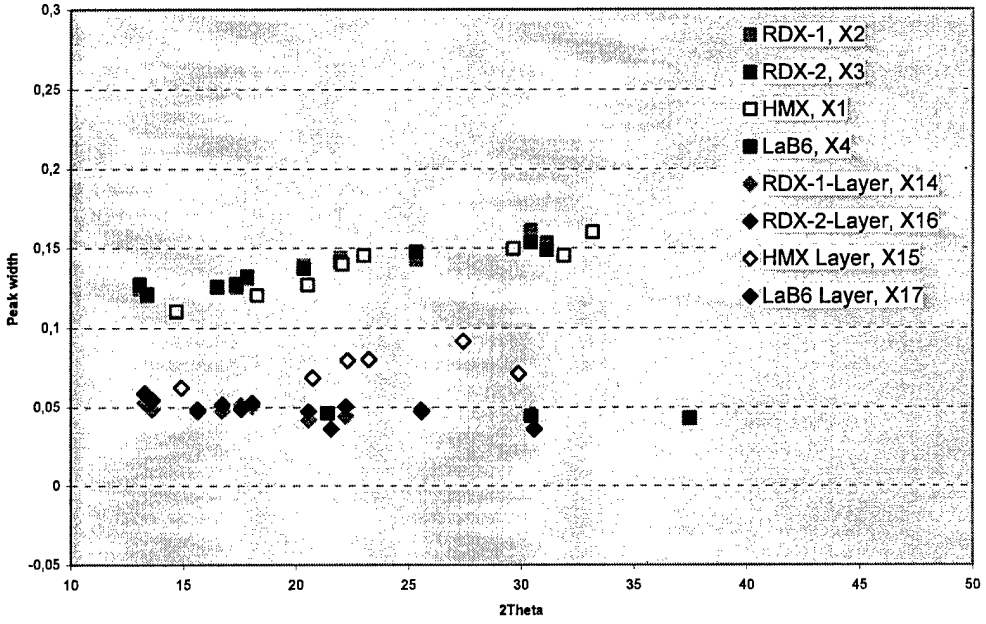


Fig. 11: FWHM of the single peaks of SRM 660a, RDX and HMX from common sample preparation and powder layers plotted versus 2Theta.

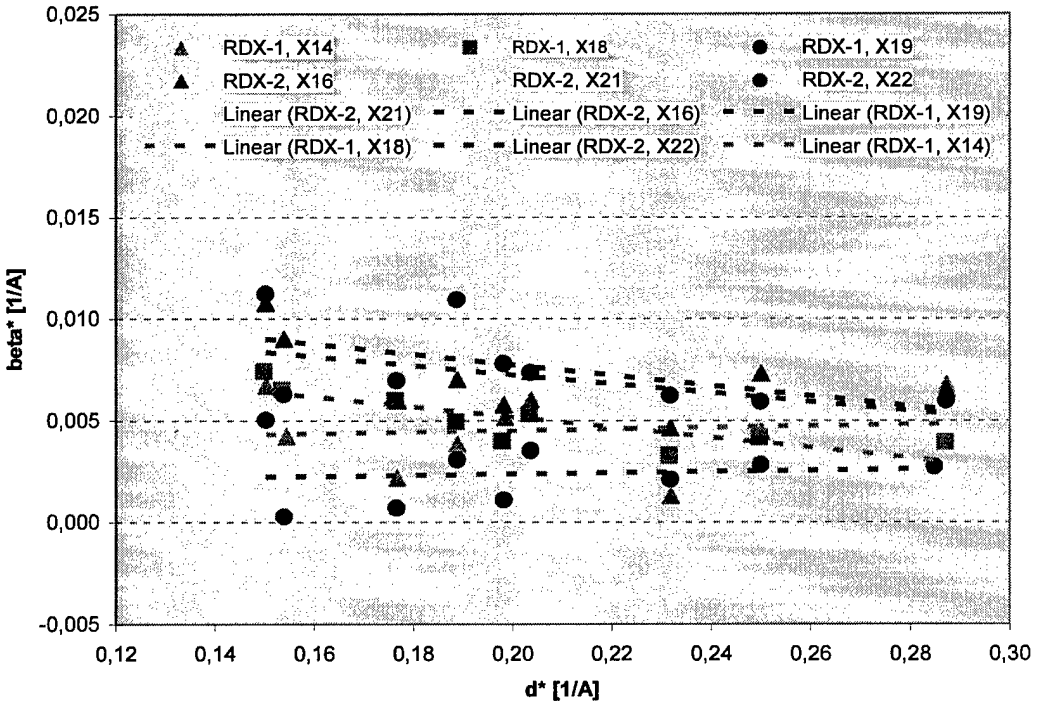


Fig. 12: Williamson-Hall-plot of RDX

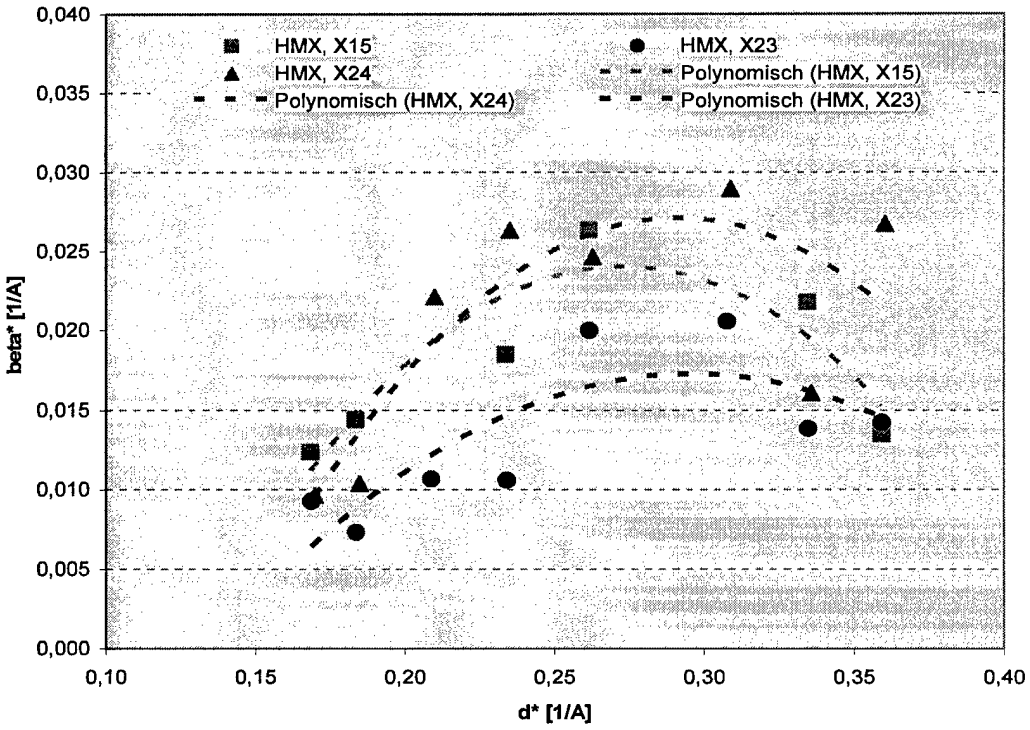


Fig. 13: Williamson-Hall-plot of HMX

Tab. 5: Regression line date from the Williamson-Hall-plots

| y=ax2+bx+c | a | b | c | $R^2$ | Mean b |
|---|---|---|---|---|---|
| RDX-1, X14 | 0 | 0.0037 | 0.0038 | 0.008 | -0.016(14) |
| RDX-1, X18 | 0 | -0.0248 | 0.0101 | 0.66 | |
| RDX-1, X19 | 0 | -0.0255 | 0.0128 | 0.31 | |
| RDX-2, X16 | 0 | -0.0221 | 0.0117 | 0.3 | -0.014(12) |
| RDX-2, X21 | 0 | -0.0229 | 0.0159 | 0.38 | |
| RDX-2, X22 | 0 | 0.003 | 0.0018 | 0.008 | |
| HMX, X15 | -1.1704 | 0.639 | -0.0632 | 0.8 | |
| HMX, X23 | -0.6704 | 0.3965 | -0.0414 | 0.64 | |
| HMX, X24 | -1.1883 | 0.6923 | -0.0737 | 0.66 | |
| < 0.33 | | | | | |
| HMX, X15 | 0 | 0.1368 | -0.0111 | 0.92 | 0.127(19) |
| HMX, X23 | 0 | 0.1001 | -0.0097 | 0.82 | |
| HMX, X24 | 0 | 0.1429 | -0.0123 | 0.79 | |

Fig. 12 and Fig. 13 show Williamson-Hall-plots of RDX and HMX and their regression lines. The regression line parameters are summarized in Tab. 5.

The RDX data admit proper fits of linear regression lines with low or even negative slopes and more or less systematic deviations around the lines. In contrast the reciprocal peak widths of HMX at first increase strongly with increasing d*, and fall down again beyond 0.33. Thus the HMX curves are better described by 2nd-order regression line, shown in Fig. 13. However, the initial slopes of the HMX-curves are well fitted by linear regressions in the d*-range below 0.33. Yielded average slopes are -0.016, -0.014 and 0.127 for RDX-1, RDX-2 and HMX, respectively. The values indicate that the micro strain is much higher in HMX then in RDX, and it seems slightly higher in RDX-2 then in RDX-1.

The average deviations of the measured data from the linear and 2nd-order regression lines of RDX and for HMX, respectively, is shown in Fig. 14 and Fig. 15. The deviations of the RDX data are systematic and significant. Low values are found for the (hkl)-reflexes with h=2 and l=0, (200), (210) and (220), high values for (111), (002) and (102).

The deviations of the HMX data are less significant. It seems that (011) and (031) are strained and (020), (11-2) and (10-2) are unstrained peaks. However the low value of (022) contradict the high one of (011), and the standard deviations indicate that the values of (10-2), (022) and (13-2) are poorly determined. Further refined investigations of HMX seem to be necessary.

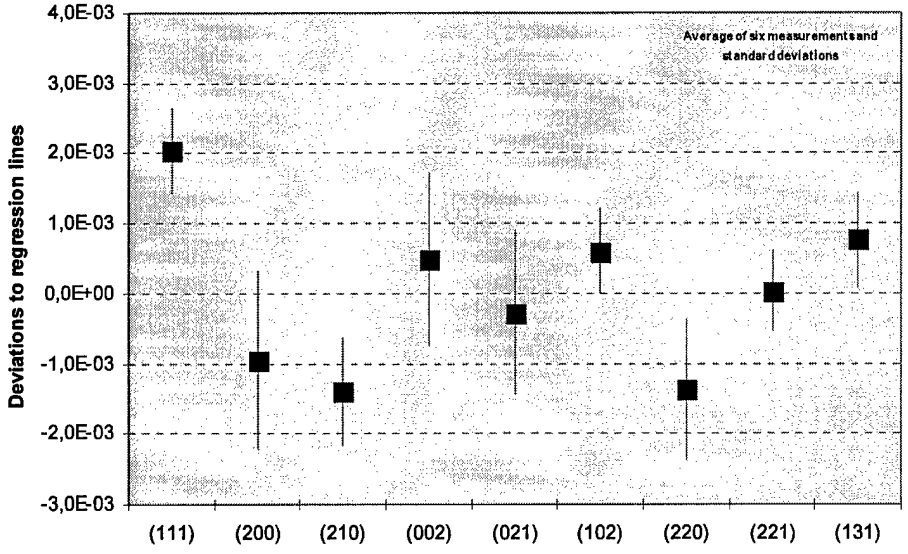


Fig. 14: Deviations of reciprocal peak widths from regression lines of RDX. Average values from six measurements.

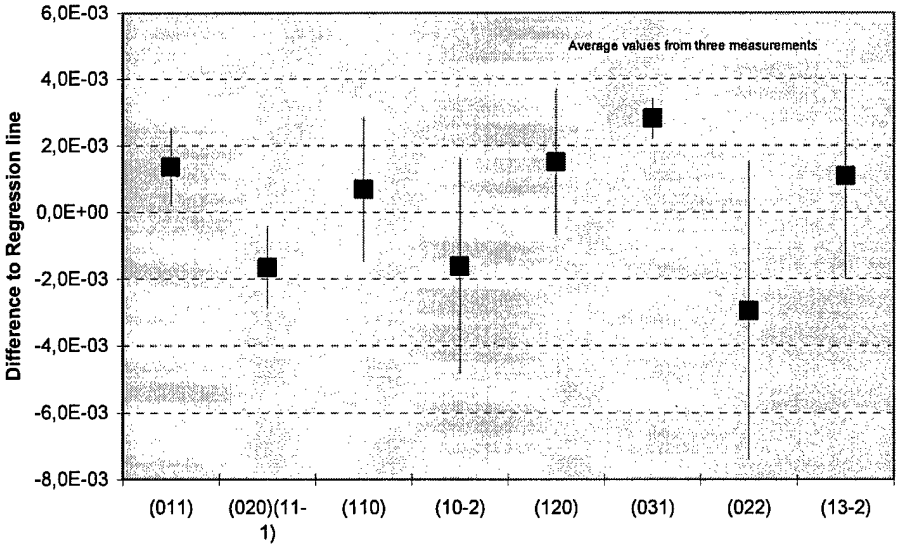


Fig. 15: Deviations of reciprocal peak widths from regression lines of HMX. Average values from three measurements.

*Fundamental parameter approach FPA*

The FPA fits as accurately as the SPVII-function. Tab. 6 summarizes the crystal size, micro strain and linear absorption coefficients evaluated from the three strongest peaks (standard deviations in brackets). The figures show a dependency of calculated crystal sizes and micro strain on the peak positions (2Theta), particularly for RDX. Average particle sizes amount to 380, 417 and 667 µm at 13.3, 13.6 and 18.1 ° 2Theta for RDX and to 273 µm for HMX, and the average micro strains amount

to 0.007, 0.006 and 0.0145 for RDX and 0.21 for HMX. The RDX-results of the measurements coincidence highly except for X21.

The results give rise for the hypothesis that the broader peaks measured with HMX stem from both, a lower crystal size and a higher micro strain. However, the accuracy of the method should be reinvestigated with further refined measurements.

Tab. 6: Crystal size, micro strain and linear absorption coefficients obtained with the fundamental parameter approach.

| | 2Theta | Aera | CrySize | MS | Abs. | Meas. |
|---|---|---|---|---|---|---|
| RDX | 13,26 | 270 | 441 | 0,0001 | 40 | X18 |
| | 13,29 | 508 | 405 | 0,0005 | 25 | X19 |
| | 13,3 | 604 | 271 | 0,0271 | 126 | X21 |
| | 13,28 | 151 | 404 | 0,0001 | 500 | X22 |
| | average | | 380(75) | 0,007(13) | | |
| | exc. X21 | | 417(21) | 0,0002(2) | | |
| | 13,59 | 122 | 466 | 0,0001 | 40 | X18 |
| | 13,62 | 236 | 489 | 0,0005 | 25 | X19 |
| | 13,63 | 290 | 275 | 0,0215 | 126 | X21 |
| | 13,61 | 71 | 440 | 0,0001 | 500 | X22 |
| | average | | 417(97) | 0,006(11) | | |
| | exc. X21 | | 465(24) | 0,0002(2) | | |
| | 18,03 | 238 | 849 | 0,0192 | 25 | X18 |
| | 18,05 | 461 | 602 | 0,0023 | 32 | X19 |
| | 18,07 | 570 | 360 | 0,0202 | 61 | X21 |
| | 18,06 | 142 | 858 | 0,0165 | 43 | X22 |
| | average | | 667(237) | 0,0145(83) | | |
| | exc. X21 | | 770(145) | 0,0127(90) | | |
| HMX | 14,95 | 513 | 481 | 0,0001 | 481 | X23 |
| | 15,03 | 347 | 279 | 0,016 | 279 | X24 |
| | 20,77 | 610 | 285 | 0,0045 | 285 | X23 |
| | 20,88 | 374 | 156 | 0,0017 | 156 | X24 |
| | 23,26 | 178 | 248 | 0,055 | 248 | X23 |
| | 23,37 | 169 | 190 | 0,046 | 190 | X24 |
| | average | | 273(114) | 0,021(24) | | |

## Discussions

The medium particle size of the fine energetic materials, determined by SEM-investigations, lie between 3 to 5 µm, where no problems with sample preparation or poor statistical distribution should occur. For that reason no special X-ray optical devices are required for the measurements of the internal crystalline properties, in contrast to earlier investigations with coarse samples.

Consequently X-ray diffraction experiments yielded continuously shaped diffraction profiles, well suited for peak profile analysis. However, the diffraction peaks of the energetic materials were strongly broadened compared to those of the reference materials. Mayor parts of the peak broadening combined with strong asymmetries represent the low absorption of the nitramines with calculated penetration depths between 600 and 650 µm.

Preparing thin powder layers reduces the penetration depth and therefore the absorption broadening. Thus much narrower peaks until 0.04 °2Theta FWHM have been obtained, even for the LaB6 with its relatively strong absorption. A further advantage has to be considered in this context. With the

relatively low symmetry of the energetic materials and the resulting high quantity of appearing peaks in the patterns, most peaks or peak tails overlap with neighboring ones. The reduction of absorption broadening yields an improved peak separation, and therefore a more reliable peak profile analysis.

However, for the high resolution poor peak intensities or long measuring time, and a relatively high underground have to be accepted. Sample holders, with lower underground in the patterns and the measurement of reduced peak ranges around the interesting peaks may moderate these lacks. Besides, the makeshift preparation of powder layers with determined reproducible thickness and the positioning of the samples have to be refined, to increase the accuracy of the method.

Common and powder layer technique revealed significant differences between HMX and RDX. The evaluation with Williamson Hall-plot and with fundamental parameter approach, point to higher micro strain in HMX compared to RDX, and the fundamental parameter approach point to a smaller crystallite size in HMX compared to RDX. Considering the defect models described in literature, dislocations in RDX and twins in HMX, it seems that twins have a stronger effect on peak broadening then dislocations. This could be discussed in terms of the different features of these defect types. Strained areas of twins are related to interfaces, whereas areas of dislocations are related to screw or edge like lines. The two-dimensional character of twins may strain a higher portion of crystals than the one dimensional of dislocations. Besides, twin interfaces separate domains and therefore may reduce the size of coherently diffracting crystallites.

A very interesting detail is the significant unisotropic peak broadening, particularly measured with the powder layer technique. The RDX peaks (111), (002) and (102) are broadened compared to (200), (210) and (220). Considering edge dislocations, broadening would occur at peaks representing net planes parallel to the edge of a dislocation, but not perpendicular. Starting with low indices [100] or [110] could represent the edge of a dislocation and [001] its burger vector. In HMX the peaks (011) and (031) are broadened compared to (020), (11-2) and (10-2). Considering twinning in HMX this could point to (011) twin planes or to unisotropic particle formation during crystallization. However, the unisotropic broadening in HMX seems to be less significant then those observed in RDX, and the results give an incomplete idea on line broadening, as only a few peaks could be separated and evaluated. No information was obtained about peaks characterizing the models given in Literature, e.g. the [-100](040) edge dislocation in RDX and (101)[10-1] twinning in HMX.

## References


Armstrong RW, Ammon HL, Du ZY, Elban WL, Zhang XJ (1993) Energetic Crystal-Lattice-Dependent Responses. in: Liebenberg DH, Armstrong RW, Gilman JJ (1993) Structure and Properties of Energetic Materials, Mat Res Soc Symp Proc Vol 296, ISBN 1-55899-191-3

Armstrong RW, Elban WL (2000) Dislocation Characteristics in Energetic Crystals; CP505, Shock Compression of Condensed Matter – 1999 edited by MD Furnish, LC Chhabildas, RS Hixon; American Institut of Physics 1-56396-923-8/00

Cady HH (1993) Growth and Defects of Explosives Crystals; Mat Res Soc Symp Prop Vol 296, 243-254

Choi CS, Prince E (1972) The crystal structure of Cyclotrimethylene-Trinitramine, Acta Cryst. B28, 2857-2862

Choi CS, Boutin HP (1970) A Study of the Crystal structure of beta-Cyclotetramethylene Tetranitramine by Neutron Diffraction, Acta Cryst B26, 1235-1240

National Institute of Standards and Technology NIST (2000) Certificate of Standard Reference Material 660a, Gaithersburg, MD 20899; Certificate Issue Date: 13 September 2000

Engel W, Herrmann M (2001) Lattice Imperfections of Energetic Materials Measured by X-ray Diffraction; Technical Report, European Research Office of the U.S. Army, Contract Number: N68171-99-M-6474

Heijden AEDM van der, Bouma RHB (1998) Shock sensitivity of HMX/HTPB PBX's: Relation with HMX crystal density; Proc 29th Int Annu Conf of ICT, 65/1-65/11

Klug PK, Alexander LE (1974) X-ray Diffraction Procedures for Polycrystalline and Amorphous Materials, Wiley, ISBN 0-471-49369-4

Kröber H, Teipel U, Leisinger K, Krause H (1998) Herstellung fehlstellenarmer Oktogenkristalle durch Rekristallisation aus Lösungen (Formation of HMX crystals with high internal quality by cooling crystallization); Proc 29th Int Annu Conf of ICT, 66/1-65/18

Palmer SJP, Field JE (1982) The deformation and fracture of b-HMX; Proc R Soc Lond A383, 399-407

Ungár T (2000) Warren-Averbach Applications, 847-867, in:
Chung FH, Smith DK (2000) Industrial Applications of X-ray Diffraction; Marcel Dekker, Inc. New York, ISBN: 0-8247-1992-1

## Acknowledgement

This material is based upon work supported by the European Office of Aerospace Research and Development, Air Force Office of Scientific Research, Air Force Research Laboratory, under Contract No. FA8655-02-M4066.

Any opinion, findings and conclusions or recommendations expressed in this material are those of the authors and do not necessarily reflect the view of the European Office of Aerospace Research and Development, Air Force Office of Scientific Research, Air Force Research Laboratory.

## Declarations

The Contractor, FRAUNHOFER INSTITUT FÜR CHEMISCHE TECHNOLOGIE., hereby declares that, to the best of his knowledge and belief, the technical data delivered herewith under Contract No. FA8655-02-M4066 is complete, accurate, and complies with all requirements of the contract.

I declare that there were no subject inventions to be declared as defined in FAR 52.227-13, during the performance of this contract.

Date: 16.12.03

(Dr. Michael Herrmann)

# Appendix

Tab. 7: Diffraction measurements and conditions

| # | Sample | System/Sample | 2Theta/Step | Time/Ch. | Rotation | File |
|---|---|---|---|---|---|---|
| X1 | HMX | BB | 5-90/0.02 | 8 s | 30 rpm | Mh071202 |
| X2 | RDX-1 | BB | 5-90/0.02 | 8 s | 30 rpm | Mh081203 |
| X3 | RDX-2 | BB | 5-90/0.02 | 8 s | 30 rpm | Mh091203 |
| X4 | LaB6 | BB | 5-90/0.02 | 8 s | 30 rpm | Mh201203 |
| X5 | RDX-1 | DS*-Capillary | 10-40/0.01 | | | Mh040603 |
| X6 | HMX | DS-Capillary | 10-40/0.01 | | | Mh050603 |
| X7 | RDX-2 | DS-Capillary | 10-40/0.01 | | | Mh060603 |
| X8 | LaB6 | DS-Capillary | 10-40/0.01 | | | Mh070603 |
| X9 | HMX | BB | 10-35/0.01 | 10 s | 30 rpm | Mh160703 |
| X10 | RDX-2 | BB | 10-35/0.01 | 10 s | 30 rpm | Mh170703 |
| X11 | RDX1 | BB | 10-35/0.01 | 10 s | 30 rpm | Mh180703 |
| X12 | RDX-1 | BB-Wafer | 10-35/0.01 | 10 s | | Mh190703 |
| X13 | RDX-1 | BB-Wafer | 10-35/0.01 | 10 s | 30 rpm | Mh200703 |
| X14 | RDX-1 | BB-Alu | 10-35/0.01 | 10 s | 30 rpm | Mh210703 |
| X15 | HMX | BB-Alu | 10-35/0.01 | 10 s | 30 rpm | Mh220703 |
| X16 | RDX-2 | BB-Alu | 10-35/0.01 | 10 s | 30 rpm | Mh230703 |
| X17 | LaB6 | BB-Alu | 10-35/0.01 | 10 s | 30 rpm | Mh240703 |
| X18 | RDX-1 | BB-Alu | 12,5-26/0.005 | 10 s | 30 rpm | Mh090903 |
| X19 | RDX-1 | BB-Alu | 12,5-26/0.005 | 10 s | 30 rpm | Mh100903 |
| X21 | RDX-2 | BB-Alu | 12,5-26/0.005 | 10 s | 30 rpm | mh110903 |
| X22 | RDX-2 | BB-Alu | 12,5-26/0.005 | 10 s | 30 rpm | mh120903 |
| X23 | HMX | BB-Alu | 14-33/0.005 | 10 s | 30 rpm | mh130903 |
| X24 | HMX | BB-Alu | 14-33/0.005 | 10 s | 30 rpm | mh140903 |
| X25 | LaB6 | BB-Alu | 14-33/0.005 | 10 s | 30 rpm | mh150903 |

*BB=Bragg-Brentano, DS=Debye-Scherrer

Tab. 8: Micro strain and crystal size of RDX and HMX obtained by fundamental parameter approach measured with common sample preparation

| RDX Position [2Theta] | hkl | Micro strain | Absorption [1/cm] | HMX Position [2Theta] | hkl | Cry Size L(nm) | Absorption [1/cm] |
|---|---|---|---|---|---|---|---|
| 13.17 | 111 | 0.0289 | 4.1 | 14.77 | 011 | 960 | 5.3 |
| 13.49 | 200 | 0.0027 | 4.1 | 18.35 | 110 | 360 | 6.9 |
| 16.61 | 002 | 0.0104 | 5.1 | 20.60 | 10-2 | 352 | 7.1 |
| 17.44 | 021 | 0.0304 | 5.1 | 22.13 | 11-2 | 175 | 7.8 |
| 17.93 | 102 | 0.0355 | 5.1 | 23.09 | 120 | 239 | 7.8 |
| 20.44 | 220 | 0.0808 | 6 | 27.27 | 031 | 240 | 6.8 |
| 22.08 | 221 | 0.0571 | 6 | 29.73 | 022 | 460 | 7.0 |
| 25.44 | 131 | 0.0301 | 6.5 | 31.98 | 13-2 | 457 | 9.0 |
| 30.51 | 322 | 0.0917 | 7.8 | | | | |

Tab. 9: Indexing (hkl) by Rietveld Analysis and selection of separated peaks (yellow) of RDX and HMX.

| RDX | | | | | | HMX | | | | | |
|---|---|---|---|---|---|---|---|---|---|---|---|
| h | k | l | d | 2Theta | int. | h | k | l | d | 2Theta | int. |
| 1 | 1 | 1 | 6,76777 | 13,071 | 1005 | 0 | 1 | 1 | 6,02244 | 14,697 | 916 |
| 2 | 0 | 0 | 6,60217 | 13,400 | 466 | 1 | 1 | -1 | 5,5278 | 16,020 | 321 |
| 0 | 2 | 0 | 5,80761 | 15,244 | 64 | 0 | 2 | 0 | 5,52402 | 16,031 | 445 |
| 2 | 1 | 0 | 5,73974 | 15,425 | 447 | 1 | 0 | 0 | 5,39711 | 16,411 | 9 |
| 0 | 0 | 2 | 5,36515 | 16,509 | 290 | 1 | 1 | 0 | 4,8494 | 18,280 | 183 |
| 0 | 2 | 1 | 5,10751 | 17,349 | 818 | 0 | 2 | 1 | 4,37901 | 20,263 | 48 |
| 2 | 1 | 1 | 5,06116 | 17,509 | 60 | 1 | 0 | -2 | 4,32364 | 20,525 | 2207 |
| 1 | 0 | 2 | 4,97052 | 17,831 | 1155 | 1 | 2 | -1 | 4,1774 | 21,252 | 0 |
| 1 | 2 | 1 | 4,76357 | 18,612 | 0 | 1 | 1 | -2 | 4,0263 | 22,059 | 175 |
| 1 | 1 | 2 | 4,56968 | 19,409 | 0 | 1 | 2 | 0 | 3,86042 | 23,020 | 1099 |
| 2 | 2 | 0 | 4,3606 | 20,349 | 821 | 0 | 0 | 2 | 3,59179 | 24,768 | 3 |
| 2 | 0 | 2 | 4,16369 | 21,323 | 48 | 0 | 1 | 2 | 3,41581 | 26,066 | 157 |
| 2 | 2 | 1 | 4,03977 | 21,985 | 590 | 1 | 2 | -2 | 3,40474 | 26,152 | 563 |
| 0 | 2 | 2 | 3,94088 | 22,544 | 119 | 1 | 1 | 1 | 3,31357 | 26,885 | 238 |
| 2 | 1 | 2 | 3,91948 | 22,668 | 11 | 0 | 3 | 1 | 3,27714 | 27,189 | 653 |
| 3 | 1 | 1 | 3,84285 | 23,127 | 49 | 2 | 0 | -2 | 3,1922 | 27,927 | 137 |
| 1 | 2 | 2 | 3,77628 | 23,540 | 109 | 1 | 3 | -1 | 3,19002 | 27,947 | 100 |
| 1 | 3 | 1 | 3,51082 | 25,348 | 705 | 2 | 1 | -2 | 3,06676 | 29,094 | 303 |
| 3 | 0 | 2 | 3,40287 | 26,167 | 76 | 2 | 1 | -1 | 3,06366 | 29,124 | 34 |
| 2 | 2 | 2 | 3,38389 | 26,316 | 30 | 1 | 3 | 0 | 3,04199 | 29,336 | 106 |
| 2 | 3 | 0 | 3,33981 | 26,670 | 0 | 0 | 2 | 2 | 3,01122 | 29,643 | 910 |
| 3 | 2 | 1 | 3,33421 | 26,715 | 155 | 1 | 2 | 1 | 2,94048 | 30,373 | 119 |
| 1 | 1 | 3 | 3,30927 | 26,920 | 527 | 1 | 3 | -2 | 2,80355 | 31,895 | 2243 |
| 4 | 0 | 0 | 3,30108 | 26,988 | 209 | 1 | 1 | -3 | 2,77989 | 32,174 | 0 |
| 3 | 1 | 2 | 3,26561 | 27,287 | 153 | 2 | 2 | -2 | 2,7639 | 32,365 | 70 |
| 2 | 3 | 1 | 3,18891 | 27,957 | 34 | 0 | 4 | 0 | 2,76201 | 32,388 | 66 |
| 4 | 1 | 0 | 3,17534 | 28,079 | 25 | 2 | 2 | -1 | 2,76163 | 32,393 | 38 |
| 1 | 3 | 2 | 3,05444 | 29,214 | 866 | 2 | 0 | 0 | 2,69856 | 33,171 | 145 |
| 0 | 2 | 3 | 3,04551 | 29,302 | 335 | 2 | 1 | -3 | 2,62732 | 34,098 | 26 |
| 4 | 1 | 1 | 3,04482 | 29,309 | 565 | 2 | 1 | 0 | 2,62149 | 34,176 | 27 |
| 2 | 1 | 3 | 3,0356 | 29,400 | 0 | 0 | 4 | 1 | 2,57802 | 34,770 | 26 |
| 1 | 2 | 3 | 2,9676 | 30,089 | 43 | 0 | 3 | 2 | 2,57131 | 34,864 | 33 |
| 3 | 2 | 2 | 2,936 | 30,421 | 386 | 1 | 2 | -3 | 2,54839 | 35,188 | 36 |
| 0 | 4 | 0 | 2,9038 | 30,766 | 168 | 1 | 4 | -1 | 2,53496 | 35,380 | 95 |
| 4 | 2 | 0 | 2,86987 | 31,139 | 266 | 1 | 3 | 1 | 2,52684 | 35,498 | 31 |
| 2 | 3 | 2 | 2,83533 | 31,528 | 92 | 1 | 4 | 0 | 2,45875 | 36,515 | 72 |
| 4 | 0 | 2 | 2,81152 | 31,802 | 11 | 2 | 2 | -3 | 2,42932 | 36,973 | 48 |
| 3 | 3 | 1 | 2,80592 | 31,868 | 157 | 2 | 2 | 0 | 2,4247 | 37,046 | 185 |
| 0 | 4 | 1 | 2,80298 | 31,902 | 188 | 1 | 0 | 2 | 2,42397 | 37,058 | 24 |
| 4 | 2 | 1 | 2,77243 | 32,263 | 516 | 2 | 3 | -2 | 2,41214 | 37,246 | 104 |
| 2 | 2 | 3 | 2,76547 | 32,346 | 339 | 2 | 3 | -1 | 2,41063 | 37,271 | 119 |
| 1 | 4 | 1 | 2,74188 | 32,632 | 0 | 1 | 1 | 2 | 2,36766 | 37,973 | 52 |
| 4 | 1 | 2 | 2,73261 | 32,746 | 83 | 0 | 1 | 3 | 2,34019 | 38,436 | 34 |
| 3 | 1 | 3 | 2,69977 | 33,156 | 302 | 1 | 4 | -2 | 2,32761 | 38,652 | 27 |
| 0 | 0 | 4 | 2,68258 | 33,375 | 70 | 1 | 3 | -3 | 2,26487 | 39,767 | 138 |
| 2 | 4 | 0 | 2,65807 | 33,692 | 59 | 1 | 2 | 2 | 2,21967 | 40,612 | 62 |
| 1 | 0 | 4 | 2,62887 | 34,077 | 122 | 0 | 2 | 3 | 2,197 | 41,050 | 83 |
| 2 | 4 | 1 | 2,58008 | 34,742 | 192 | 0 | 4 | 2 | 2,1895 | 41,197 | 205 |